# A MODIFIED COMPRESSIBLE SMOOTHED PARTICLE HYDRODYNAMICS (MCSPH) METHOD AND ITS APPLICATION ON THE NUMERICAL SIMULATION OF LOW AND HIGH VELOCITY IMPACTS

**N. Amanifard**\* **and V. Haghighat Namini**

*Mechanical Engineering Department, Faculty of Engineering, University of Guilan, Rasht, P.O. Box 3756, Iran*
*namanif@Guilan.ac.ir, vahab.haghighat@gmail.com*

\*Corresponding Author

**Abstract**    In this study a Modified Compressible Smoothed Particle Hydrodynamics (MCSPH) method is introduced which is applicable in problems involving shock wave structures and elastic-plastic deformations of solids. As a matter of fact, algorithm of the method is based on an approach which descritizes the momentum equation into three parts and solves each part separately and calculates their effects on the velocity field and displacement of particles. The most exclusive feature of the method is exactly removing artificial viscosity of the formulations and representing good compatibility with other reasonable numerical methods without any rigorous numerical fractures or tensile instabilities while MCSPH does not use any extra modifications. Two types of problems involving elastic-plastic deformations and shock waves are presented here to demonstrate the capability of MCSPH in simulation of such problems and its ability to capture shock. The problems that are proposed here are low and high velocity impacts between aluminum projectiles and semi infinite aluminum beams. Elastic-perfectly plastic model is chosen for constitutive model of the aluminum and the results of simulations are compared with other reasonable studies in these cases.

**Keywords:** Smoothed Particle Hydrodynamics, Modified algorithm, Low velocity impact, High velocity impact.

چکیده   در مطالعه حاضر، یک روش بهبودیافته هیدرودینامیک ذره هموار تراکم‌پذیر (MCSPH) معرفی می‌گردد که در مسائل  ساختارهای موج شوک و تغییر شکل‌های الاستیک–پلاستیک در جامدات کاربرد دارد. در حقیقت، الگوریتم این روش بر اساس دیدگاه جداسازی معادله مومنتوم به سه بخش مجزا و حل جداگانه هر بخش و محاسبه تاثیرات آنها بر میدان سرعت و جابجایی ذرات بنا نهاده شده‌است.ویژه‌ترین خصوصیت این روش، حذف لزجت مصنوعی از فرمول‌بندی‌های آن و ارائه هماهنگی مناسب با دیگر روش‌های معتبر عددی، بدون هیچ شکست عددی مهم یا ناپایداری کششی است. این در حالی است که در روش حاضر از هیچ‌گونه اصلاحی استفاده نمی‌شود. در این جا دو نوع مسئله شامل تغییر شکل‌های الاستیک – پلاستیک و موج‌های شوک ارائه می‌گردد تا توانایی روش MCSPH را در شبیه‌سازی چنین مسائلی و در تسخیر شوک نشان دهد. مسائل ارائه شده در این مطالعه، ضربه‌ها، ضربه‌ها (برخوردها)ی سرعت پایین و سرعت بالا بین پرتابه‌ها و تیرهای نیمه بی‌نهایت آلومینیومی هستند. مدل الاستیک– کاملاً پلاستیک برای مدل ساختاری آلومینیوم انتخاب شده‌است و نتایج شبیه‌سازی‌ها با نتایج مطالعات معتبر دیگر مورد قیاس قرار گرفته‌اند.

## 1. INTRODUCTION

Smoothed particle hydrodynamics (SPH) is a Lagrangian particle method, or, in other words, is a gridless technique that competes with conventional Lagrangian and Eulerian mesh based techniques. Advent of SPH is related to solution of Astrophysical problems [1, 2, 3], free surface problems [4], problems with large deformation such as high velocity impact of solids [5], impact between solid and fluid [6], chemical explosions [7] and fracture of solids [8] .

Through the large deformations, formal grid-based techniques have trouble with grid

entanglement, and require complicated regridding procedures to deal with this problem. But in SPH, this problem is not the major problem and the nature of the interpolation, the basic approach of SPH, eleminates this trouble. In SPH, fields of velocity, pressure and so on, are related to particles. The word 'particle' does not mean a physical mass, but instead, it refers to a region in space. Field variables are associated with these particles and at any other point in space are found by averaging, or smoothing the particle values over the region of interest. This is satisfied by an interpolation or weight function which is usually called the interpolation Kernel [1].

SPH has different formulations, but the essential difference between these formulations is related to problems involving shock wave structures, is how they deal with shock capturing problem. The problem is that real shocks are very thin discontinuities in the solution, and hence they make some noises in computations. In the most instances of the use of the SPH, for controlling the oscillations around shocks, artificial viscosity (**AV**) are used [2].

As mentioned above, most of previous numerical SPH simulations of high or low velocity impacts with techniques, were faced with numerical fracture or tensile instabilities as well as clumping of particles in high tensile regions, during the solution steps, and to avoid such difficulties, each of them proposed their own artificial viscosity, equation of state, and extra modifications such as artificial stress. Briefly, the main goal of current work is to introduce a new solution algorithm without the requirements of using the artificial viscosity (**AV**), and minimizing the solution modification factors. This technique is named Modified Compressible SPH (MCSPH).

## 2. FUNDAMENTALS OF SPH

The SPH method is based on the interpolation theory. The method permits any function to be expressed in terms of its values at a set of disordered points representing particle positions using kernel function. The kernel function refers to a weighting function and specifies the contribution of a typical field variable, $f(r)$, at a certain position , $r$, in space. The kernel estimation of $f(r)$ is defined as [14]:

$$\langle f(r) \rangle = \int f(r')W(r-r',h)dr' \tag{1}$$

The smoothing length $h$ represents the effective width of the kernel and $W$ is a weighting function with following conditions:

1. $W$ must reduce to a delta function in the limit of small smoothing length

$$\lim_{h \to 0} W(r-r',h) = \delta(r-r') \tag{2}$$

2. $W$ must be normalized

$$\int W(r-r',h)dr' = 1 \tag{3}$$

Employment of a kernel function transforms the partial differential equations of continuum dynamics into integral equations through the kernel estimation (Equation 1).

The integral is discretized to a sum over particles, i.e.

$$\langle f(r_i) \rangle \approx \sum_{j=1}^{N} m_j f_j W(r_i - r_j, h) / \rho_j \tag{4}$$

Here, $m_j$ is the mass and $\rho_j$ is the density associated with the $j_{th}$ particle, and $f_j = f(r)_{r=r_j}$. Integrating the above equation by parts and using the compactness property of $W$, we get an expression for the derivative.

$$\langle \nabla f(r_i) \rangle_{r=r_i} \approx -\sum_{j=1}^{N} m_j f_j \nabla_j W(r_i - r_j, h)_{r=r_j} / \rho_j \tag{5}$$

These equations yield estimates for accelerations, strain and so on.

**2.1. The Kernel Function** The kernels used in the SPH method approximate a delta function. Monaghan [8] proposed a compact support condition for suitable kernel to guarantee zero interactions outside its computational domain. The original calculations of Gingold and Monaghan [9] used a Gaussian Kernel. Although this kernel, satisfies the basic requirements given by equations (1), and (2), it does not possess a compact support so its computational efficiency is rather low[10]. Various other forms of the kernel function such as

super-Gaussian [11], Spline [12], and polynomial [13] kernels and so on, were proposed later. Recent studies [8, 14], indicate that the stability of the SPH algorithm depends strongly upon the second derivative of the kernel. One of the most popular kernels based on Spline functions [8] is named Cubic Spline and defined as:

$$W(r,h) = \frac{\sigma}{h^m} \begin{cases} 1 - \frac{3}{2}z^2 + \frac{3}{4}z^3 & 0 \le z < 1 \\ \frac{1}{4}(2-z)^3 & 1 \le z < 2 \\ 0 & 2 \le z \end{cases} \qquad (6)$$

where, $z = |r|/h$, $m$ represents the number of dimensions and $\sigma$ is normalization constant which takes the values 2/3, $10/7\pi$, $1/\pi$ in one, two and three dimensions. This kernel has compact support so that its interactions are exactly zero for $r > 2h$.

**2.2 Fundamental Operators in SPH** With regards to principal equations of the method, some calculus operators such as first derivatives, gradient, and divergence are needed to be rearranged in SPH discretized forms [15]. First order derivatives in SPH forms are:

$$(\frac{\partial v}{\partial x})_i = \sum_j \frac{m_j}{\rho_j}(v_j - v_i)\frac{x_i - x_j}{|r_{ij}|}\frac{dW}{dr_{ij}} \qquad (7)$$

$$(\frac{\partial v}{\partial y})_i = \sum_j \frac{m_j}{\rho_j}(v_j - v_i)\frac{y_i - y_j}{|r_{ij}|}\frac{dW}{dr_{ij}} \qquad (8)$$

where, $r_{ij} = r_i - r_j$. Other derivatives can be calculated in the same way. The gradient of a scalar $A$ and divergence of vector $\vec{v}$ are represented as:

$$\frac{1}{\rho_i}\nabla_i A = \sum_j m_j(\frac{A_i}{\rho_i^2} + \frac{A_j}{\rho_j^2})\nabla_i W_{ij} \qquad (9)$$

$$\frac{1}{\rho_i}\nabla_i \cdot \vec{v}_i = \sum_j m_j(\frac{\vec{v}_i}{\rho_i^2} + \frac{\vec{v}_j}{\rho_j^2}) \cdot \nabla_i W_{ij} \qquad (10)$$

where $\nabla_i W_{ij}$ is the gradient of the kernel function $W(r_i - r_j, h)$: here $\vec{r_i}$ is the position vector of the particle $i$.

## 3. THE GOVERNING EQUATIONS

The basic equations of a continuum mechanics expressing conservation of mass, momentum and energy are represented as following [16]:

$$\frac{d\rho}{dt} = -\rho\nabla \cdot \vec{v} \qquad (11)$$

$$\frac{d\vec{v}}{dt} = \frac{1}{\rho}\nabla \cdot \sigma \qquad (12)$$

$$\frac{de}{dt} = \frac{1}{\rho}\sigma \cdot \nabla\vec{v} \qquad (13)$$

where $d/dt$ means the substantial derivative, $\rho$ is the density, $e$ is the internal energy per unit mass, and $\sigma$ is the Cauchy stress tensor.

Rearranging the above equations in SPH discretized forms by using Equations (7) to (10), and using the conventional SPH method [16, 17] and [17] that adds the artificial viscosity $\Pi ij$, the formulations become:

$$\frac{d\rho_i}{dt} = \rho_i \sum \frac{m_j}{\rho_j}(v_i - v_j) \cdot \nabla W_{ij}, \qquad (14)$$

$$\frac{dv_i}{dt} = -\sum m_j\left(\frac{\sigma_i}{\rho_i^2} + \frac{\sigma_j}{\rho_j^2} + \Pi_{ij}I\right) \cdot \nabla W_{ij}, \qquad (15)$$

$$\frac{de_i}{dt} = \frac{1}{2}\sum_j m_j(v_j^\alpha - v_i^\alpha)(\frac{\sigma_i^{\alpha\beta}}{\rho_i^2} + \frac{\sigma_j^{\alpha\beta}}{\rho_j^2} - \Pi_{ij})W_{ij},\beta \qquad (16)$$

where ($\alpha$, $\beta = 1$, 2) are the nominators of the spatial coordinates and $W_{ij},\beta = \partial W_{ij}/\partial x_i^\beta$ is the derivative of the kernel function $W$ with respect to position vector $x$ of the $i_{th}$ particle.

In current work, the basic equations of the system in the following from are more suitable for the MCSPH instead of general forms of Equations (11) to (13):

$$\frac{1}{\rho}\frac{d\rho}{dt} + \nabla \cdot \vec{v} = 0 \qquad (17)$$

$$\frac{d\vec{v}}{dt} = \vec{g} + \frac{1}{\rho}\nabla \cdot \vec{S} - \frac{1}{\rho}\nabla P \qquad (18)$$

$$\frac{de}{dt} = \frac{1}{\rho}\sigma.\nabla\vec{v} \qquad (19)$$

where $t$ is time, $\vec{g}$ is gravitational acceleration, $P$ is pressure, $\vec{v}$ is the velocity vector, $\vec{S}$ is the deviatoric part of the Cauchy stress tensor $\sigma$ and $d\vec{v}/dt$ refers to the material derivative, in which stokes theorem is used to segregate the stress tensor to viscous and pressure parts in momentum equations.

The main difference between the current method and the conventional SPH methods is in solution steps regarding the rearranged form of the momentum equations (Eq. 18). A similar solution technique is proposed by Hosseini et al. [15]. Their technique is incompressible while MCSPH is compressible which is suitable for problems involve shock wave structures.

Previously, Hosseini algorithm was used to simulate fluid structure interaction [18] and high velocity impact problem without shock capturing [19]. With These simulations, it is evident that Hosseini algorithm is a reliable algorithm of SPH, especially in incompressible physics. But shock capturing ability is vital for those who want to simulate impact problems. In this paper, it is focused to show the ability of the new modified three step compressible algorithm (MCSPH) in the field of shock capturing.

## 4. ARTIFICIAL VISCOSITY

In order to simulate problems of hydrodynamics, special treatments or methods are required to allow the algorithms to be capable of modeling shock waves, or else the simulation will develop unphysical oscillations in the numerical results around the shocked region. A shock wave is not a true physical discontinuity, but a very narrow transition zone whose thickness is usually in the order of a few molecular mean free paths. To capture shock wave, it is needed to damp and control oscillations around shock wave structures [20]. So, in conventional SPH algorithms a term named artificial viscosity has been added to momentum equation to overcome unwanted oscillations around shock waves. The artificial viscosity terms are usually added to the physical pressure term, and help to diffuse sharp variations in the flow and to dissipate the energy of high frequency term. The SPH method was first applied

to treat problems with low or no dissipation. Later an artificial viscosity was developed [21] to allow shocks to be simulated. This Monaghan type artificial viscosity $\Pi ij$ is the most widely used artificial viscosity so far in the SPH literature. The detailed formulation is:

$$\Pi_{ij} = \begin{cases} \dfrac{-\alpha_{\Pi}\bar{c}_{ij}\varphi_{ij}^2}{\bar{\rho}_{ij}} & v_{ij}.x_{ij} < 0 \\ 0 & v_{ij}.x_{ij} > 0 \end{cases} \tag{20}$$

$$\phi_{ij} = \frac{h_{ij}v_{ij}.x_{ij}}{\left|x_{ij}\right|^2 + \phi^2} \tag{21}$$

where, $\bar{c}_{ij}$, $\bar{\rho}_{ij}$ and $\bar{h}_{ij}$ are, mean values of sound speed, density and smoothing length between $i_{th}$ and $j_{th}$ particles, respectively. Also $\alpha_{\Pi}$ and $\beta_{\Pi}$ are constants about 0.1 and the factor $\phi = 0.1h_{ij}$ is inserted to prevent numerical divergences when two particles are approaching each other [24].

One of the purposes of the current study is to eliminate artificial viscosity from SPH formulations which is not a primary component of momentum equation and relieve the oscillations around shock wave structures with changing the structure of SPH conventional algorithms.

## 5. SOLUTION ALGORITHM

In section 3, all the necessary operators for discretizing Equations (17) to (19) are defined. The three parts in right hand side of Equation (18) suggestthat the momentum equation can be solved in three steps. At the first step the velocity variations are related to the body force, and the computed results are saved to the temporary variable ($\vec{v}^*$).

$$\frac{d\vec{v}^*}{dt} = \vec{g} \tag{22.1}$$

And,

$$\vec{v}^* = \vec{v}_{t-\Delta t} + \vec{g}\Delta t \tag{22.2}$$

This step is actually valuable for the physics that

the body force has a significant role in deformations, whereas in impact studies it is ignorable.

In the second step, the velocity vector ($\vec{v}$) is confronted with the deviatory stress tensor ($\vec{S}$), and the computed results are saved to the second temporary variable ($\vec{v}^{**}$), and as a result a temporary position vector of the particles ($\vec{r}^*$) is related to this temporary velocity:

$$\left(\frac{1}{\rho}\nabla\cdot\vec{S}\right) = div\vec{S} = S_x i + S_y j \tag{23.1}$$

Regarding the momentum equation:

$$\vec{v}^{**} = \vec{v}^* + div\vec{S}\Delta t \tag{23.2}$$

And,

$$\vec{r}^* = \vec{r}_{t-\Delta t} + \vec{v}^{**}\Delta t \tag{23.3}$$

After this step, the conservation of mass is checked by replacing the computed velocity vectors in the continuity equation (Eq. 17), and a temporary value ($\rho^*$) is found for the $\rho$:

$$\rho^* = \rho - (\rho\nabla\cdot\vec{v})\Delta t \tag{24}$$

At the final step, the algebraic equation of state, which is expressed in the form of $P = P(\rho,e)$ is solved, and the pressure field is updated. The updated pressure is used to correct the temporary velocity and the position of the particle:

$$\hat{\vec{v}} = -(\frac{1}{\rho}\nabla P)\Delta t \tag{25.1}$$

$$\vec{v}_t = \vec{v}^{**} + \hat{\vec{v}} \tag{25.2}$$

$$\vec{r}_t = \vec{r}_{t-\Delta t} + \frac{\Delta t}{2}(\vec{v}_t + \vec{v}_{t-\Delta t}) \tag{25.3}$$

$$\rho = \rho^* \tag{25.4}$$

With the new values for principle variables at this moment, it is possible to derive Cauchy stress tensor by aggregating the values of deviatory stress and pressure, for solving the equation of energy in a fully explicit manner. Thereby, solving the

equation of energy, a new value for internal energy per unit mass of each particle would be obtained. This new value for specific internal energy can be used as an initial value at the next time step for solving the equation of state.

Other necessary equations can be solved same as the energy equation at this stage, with a fully explicit approach in the time marching.
Now, all the required computations for a single time step are completed.

The main difference of the current algorithm with that proposed by Hosseini, et al. [15] stands on density variations. In this study, the continuum is compressible whereas Hosseini, et al. [15] used the incompressible approach and did not use the equation of state. As a result, the current algorithm inherently has the capability of shock capturing, which plays an important role in plastic deformations.

## 6. CONSTITUTIVE EQUATIONS

**6.1. Isotropic Material** For an isotropic material the Cauchy stress tensor in Equation (19) is defined in terms of deviatory stress $S^{\alpha\beta}$ and pressure **P**, as follows:

$$\sigma^{\alpha\beta} = S^{\alpha\beta} - \delta^{\alpha\beta}P \tag{26}$$

where, $\delta^{\alpha\beta}$ is the Kronecker delta. To account for the rotation effect caused by the large deformation of the material, the elastic deviatoric stress rate $\dot{S}^{\alpha\beta}$ using the Jaumann rate is given as follows [23]:

$$\dot{S}^{\alpha\beta} = 2\mu(\dot{\varepsilon}^{\alpha\beta} - \frac{1}{3}\delta^{\alpha\beta}\dot{\varepsilon}^{\alpha\beta}) + S^{\alpha k}\Omega^{\beta k} + \Omega^{\alpha k}S^{k\beta} \tag{27}$$

where $\dot{\varepsilon}^{\alpha\beta}$ are strain rates.

$$\dot{\varepsilon}^{\alpha\beta} = \frac{1}{2}(\frac{\partial v^\alpha}{\partial x^\beta} + \frac{\partial v^\beta}{\partial x^\alpha}) \tag{28}$$

and $\Omega^{\alpha\beta}$ denotes the rotation:

$$\Omega^{\alpha\beta} = \frac{1}{2}(\frac{\partial v^\alpha}{\partial x^\beta} - \frac{\partial v^\beta}{\partial x^\alpha}) \tag{29}$$

The rotation terms ensure invariance between rotated observer frames for small deformations [22]. Regarding Equations (17), (18) and (19), one

needs to have pressure to gain the total stress in each particle for solving momentum and energy equations. As explained, the equation of state (EOS) in the form of $P = P(\rho, e)$ is used to compute the pressure.

The desired equation of state used in current work is Mie-Grunisen EOS [18]:

$$P(\rho, e) = (1 - \frac{1}{2}\Gamma\eta)P_H(\rho) + \Gamma\rho e \qquad (30)$$

where $\Gamma$ is The Grunisen constant, $\eta = (\frac{\rho}{\rho_0} - 1)$ is the parameter which represents the compressive behavior, $\rho_0$ is the initial density, and $P_H$ is the so-called Hugoniot curve commonly used in the SPH method, and is written as:

$$P_H = \begin{cases} a_1\eta + a_2\eta^2 + a_3\eta^3 & for\ \eta > 0 \\ a_1\eta & for\ \eta \leq 0 \end{cases} \qquad (31)$$

In Equation (31), the constants $a_1$, $a_2$ and $a_3$ can be expressed in terms of the parameters $C_0$ and $\xi$ which appear in the linear relation of the shock velocity $\vec{v}_s$ and particle velocity $\vec{v}_p$, i.e. $\vec{v}_s = c_0 + \xi\vec{v}_p$, as

$$a_1 = \rho_0 c_0^2 \qquad (32.1)$$

$$a_2 = a_1[1 + 2(\xi - 1)] \qquad (32.2)$$

$$a_3 = a_1[2(\xi - 1) + 3(\xi - 1)^2] \qquad (32.3)$$

**6.2. Elastic-Perfectly Plastic Model** It is a well known fact that the materials are not perfectly elastic, and if the applied stress exceeds a critical value the material starts its plastic behavior. The von-Misses yielding criterion is used to compute the critical stress. So, deviatory stress tensor is limited [24]:

$$S^{\alpha\beta} \Rightarrow fS^{\alpha\beta} \qquad (33)$$

where $f$ is computed from:

$$f = \min\left[\frac{Y_0^2}{3J_2}, 1\right] \qquad (34)$$

where $J_2$ is the second invariant of the deviatoric stress tensor defined by:

$$J_2 = \frac{1}{2}S^{\alpha\beta}S^{\alpha\beta} \qquad (35)$$

and $Y_0$ is a material dependent yield stress which is in general $Y_0 = Y_0(T, \rho, ...)$.

## 7. TEST CASES

Two different test cases are simulated by MCSPH method, and a FORTRAN 95 code is provided to solve the equations. In both test cases all the domain are simulated and symmetry conditions are not used.

**7.1. 2D-Low Velocity Impact** Here, an aluminum projectile with the velocity of 400 (*m/s*) strikes into a semi infinite aluminum target, the same as the case of Howell et al. [25] with exactly the same features. The material properties are shown in Table 1.

**TABLE 1.** Material Properties for Aluminum

| Property | Value |
|---|---|
| Density, $\rho$ ( $kgm^{-3}$ ) | 2785 |
| Bulk sound speed, $C_0$ ( $ms^{-1}$ ) | 5328 |
| Gruneisen modulus, $\eta$ | 2.0 |
| Shear modulus, $\mu$ ( $pa$ ) | $2.76 \times 10^{10}$ |
| Yield stress, $Y_0$ ( $pa$ ) | $3.0 \times 10^8$ |

Fig. 1 shows the initial configuration of the problem. The dimensions of the projectile are set to $0.50 \times 10^{-2}$ (*m*), $1.20 \times 10^{-2}$ (*m*) and for the target are set to $2.20 \times 10^{-2}$ (*m*) and $3.80 \times 10^{-2}$ (*m*) respectively.

To decrease the computational efforts the initial length for the particles of the projectile is set to be constant, and similarly, two different initial constant lengths are set for particles of the target. At the interface zone, the particles are smaller than particles in outer zones. The total number of the particles in computational domain is 13676. The problem is solved for 3.0 (*μs*) after the initial contact between the projectile and the target. The computed results are compared with the same problem which is solved by Howell and Ball [9] in two different methods.
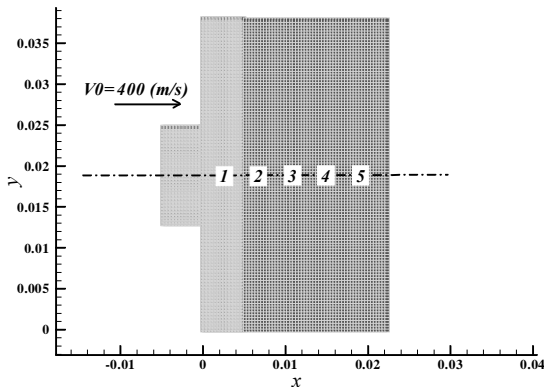
**Figure 1.** The initial configuration of the low velocity impact with initial projectile velocity of 400 (*m/s*)

Howell et al. [25] modeled the impact a free Lagrange augmented Godunov method (that is called free Lagrange method in this study), and then solved it with AUTODYN SPH code. Fig. 2 shows the contribution of the total x-wise stress in the both the projectile and the target in 4 different time steps. In comparison with Howell and Ball [25], it is apparent that the current computed results are in a good agreement with the referred works. Figure 2 also illustrates the wave generated in the projectile and the target at 0.5, 1.0, 2.0 and 3.0 (*μs*) after initial contact.

At 0.5 (*μs*), shock waves were generated at the interface and also were propagated toward both sides, back into the projectile, and rightward into the target. At 1.0 (*μs*), because of the shock reflections at the lower and upper free surfaces of the projectile, rarefaction waves were originated and meet at the symmetry axis. The left-running shock wave has also reached the rear of the projectile and has reflected as a rarefaction. After 2.0 (*μs*), the two-wave family has matured and an elastic precursor wave and trailing plastic shock have formed. The rarefaction returned from the rear of the projectile has crossed into the target, and produced a region of high tensile stress in the *x*-direction that is approximately $1.82 \times 10^9$ (*pa*) which is close to the Howell and Ball's [25] $1.9 \times 10^9$ (*pa*) at this region. At the final elapsed time of 3.0 (*μs*), wave structures have reached the top and bottom of the target and the plastic shock was started to be weakened. Deformation of both the projectile and the target is obvious at the interface, top and bottom of the projectile. At the second part of this study, as shown in Fig. 1, five

distinct points are chosen to be analyzed. Point 1 is initially 1.8125 mm from the face contact and x-wise distance between points is 3.625 mm. Figure 3 shows the time histories of pressure, density, x-wise velocity and the total stress in x-wise direction, which are recorded at these points, and are compared with the results of Howell et al. [25].

It is apparent that the MCSPH method has the required capability of shock capturing considering the good agreement between compared data.
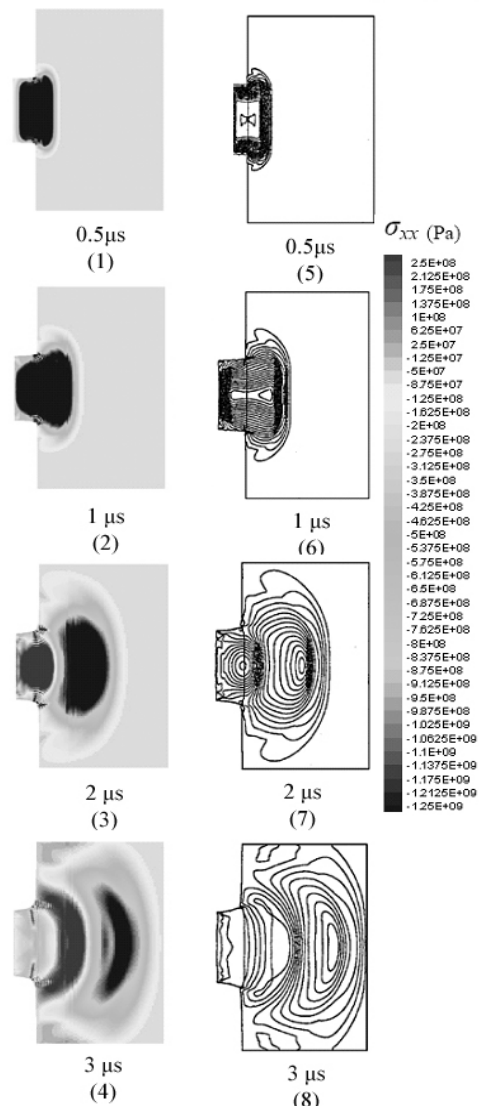


**Figure 2.** Four different time intervals of low velocity impact problem. Figs. 1 to 4 is related to MCSPH simulation and Figs. 5 to 8 is related to AUTODYN free Lagrange solver of Howell & Ball [25] with total x-wise stress interval of 150 (*Mpa*).
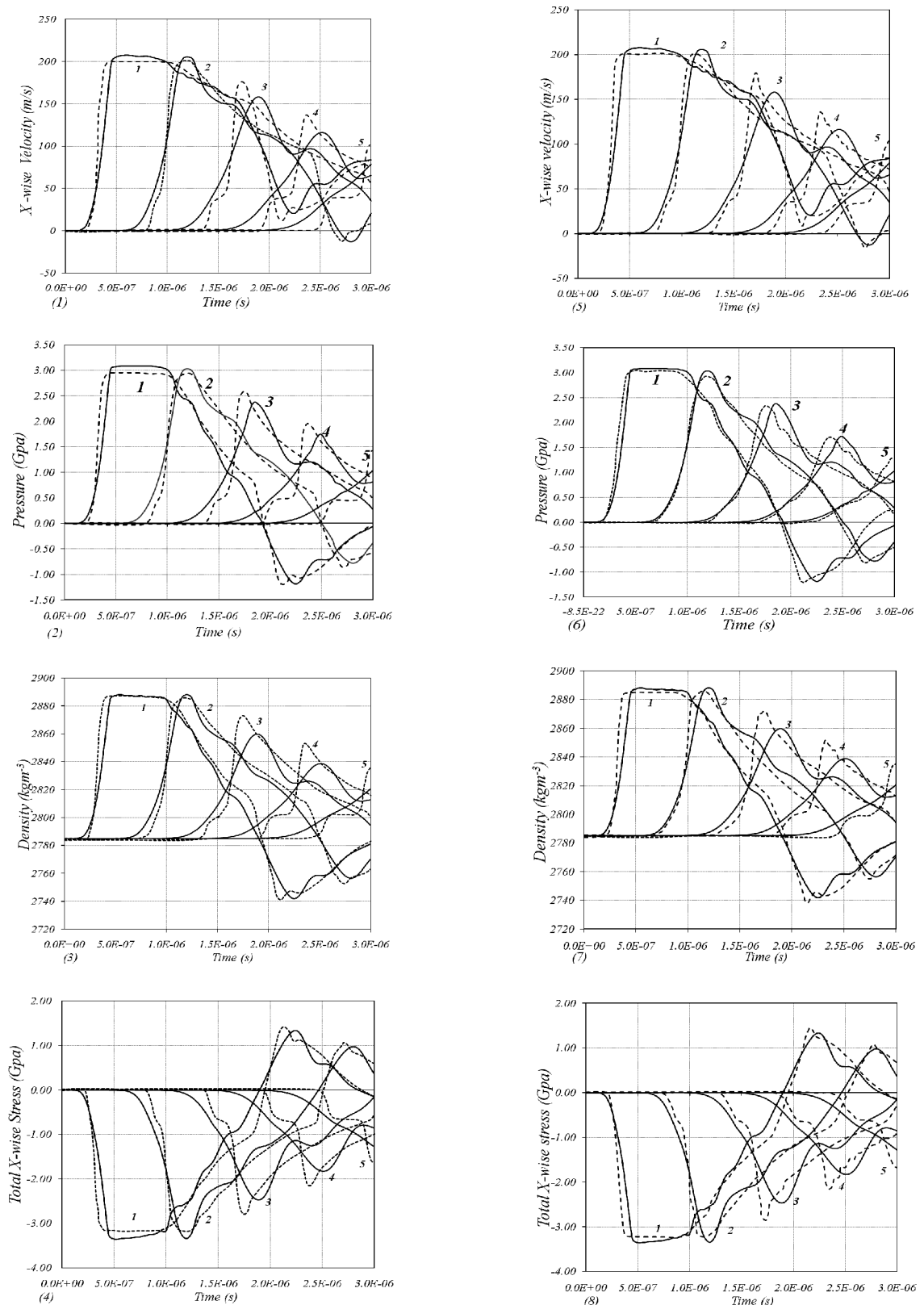
**Figure 3.** Time variation of four main parameters at 5 distinct points (Illustrated in Figure 1). Diagrams 1 to 4 are related to MCSPH in comparison with Free Lagrange solver of the Howell et al. [25] and diagrams 5 to 8 are related to MCSPH in comparison with SPH solver of the Howell et al. [25].In each Diagram, solid lines show the results of current study (MCSPH) and dash lines imply to Results of Howell et al. [25].

Because of the explicit nature of the method and elimination of artificial viscosity (**AV**), in some cases more damping in pressure and other variables that are shown in the Figure 3 during the solution are observed, in comparison with AUTODYN SPH code and Free Lagrange method used in Howell and Ball [25], but in general, it has a good compatibility in shock capturing and amplitude of shock waves specially when compared with SPH solver of Howell and Ball [25].

**7.2. 2. D-High Velocity Impact** The second test case is the solution of a high velocity aluminum-aluminum impact (3.1 *km/s*). In this case, it is expected that the pressure has a bigger magnitude than yield strength of the material and however, a localized fluid-like plastic behavior is also expected when the case is compared to the low velocity case.

In Fig. 4, initial position of the aluminum target and the projectile is shown. The impact velocity is set to 3.1 (*km/s*). The dimensions and the other characteristic of both the target and the projectile are the same as the case of Howell et al. [25].

Diameter of the circular projectile is 10.0 mm and the target has 2.0 mm width and 50.0 mm height. However, 12046 particles are used to simulate the physic, 5406 of which in the projectile and 6640 in the target ($\Delta$L= initial particle length =0.12 *mm*). The results are checked with the woks of Howell et al [25] and Mehra et al. [16].

In Fig. 5, transient results for an elapsed time of 8.0 ($\mu s$), after contact of the projectile to the target are shown. In this figure pressure contribution for both the projectile and the target is shown in 8 different Figs. 1- 8. It is apparent that the shocks are captured and the results are in good agreement with Howell et al. [25] in arrival time of the waves, and in magnitude of pressure. The pressure at the centre of the projectile, behind the leftward running shock, after 1.0 ($\mu s$), (Fig. 5.1) is recorded as $18.72 \times 10^9 (pa)$ that is clearly close to $18.6 \times 10^9 (pa)$ of Howell et al. [25] at the same time and in the same position. Noticeable deformation of both the target and the projectile are seen at 2.0 ($\mu s$), with thin arms of ejecta released from the front face of the target (Fig. 5.2). It is noticeable in Figs. 5.2 and 5.3 that a region of a strong tension has been generated at the rear face of the projectile, because of the reflection of the focused wave structures.
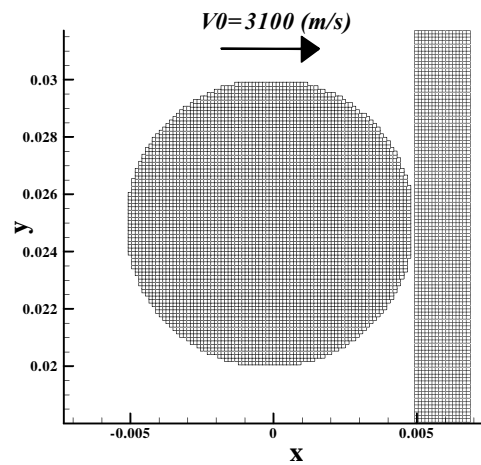


**Figure 4.** The initial configuration of high velocity impact problem with projectile initial velocity of 3.1 *km/s*.

A tensile pressure of $-16.62 \times 10^9 (Pa)$ is noted in the core of the wave structure. These values are checked in Table 2 with values of both Howell et al. [25] and Mehra et al. [16] studies. At 1.0 ($\mu s$), the most part of this wave reflects as a compression wave, and it reaches the target from the projectile and then reflects again as a tensile wave. This procedure is repeated in other time intervals. Consequently, in every reflection, wave is weakened and loses its power. During this process, the arms of the ejecta get larger and in about 2.0 ($\mu s$), begin to break away from the front of the target. Throughout the process, large deformation is exerted in both the projectile and the target, especially in the projectile and at the interface.

On the other hand, the more the projectile penetrates into the target, the more reduction in resistance of the target is created and the projectile goes ahead and carries the target particles with itself till a narrow region remains around the projectile with a little resistance against the projectile's momentum. Results show that the current method is a convenient and practical method in high velocity impact and large deformation problems. It is in a good agreement with other valuable studies accomplished by other researchers such as Howell et al. [25] and Mehra et al. [16].
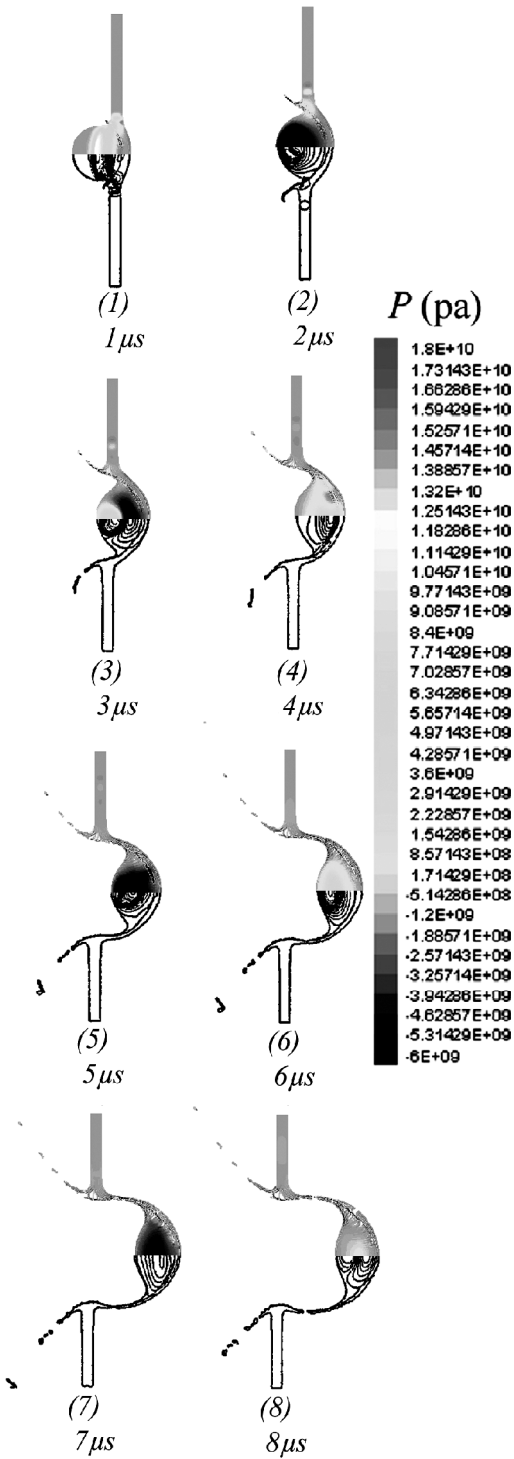
(1) 1 μs   (2) 2 μs

P (pa)

1.8E+10
1.73143E+10
1.66286E+10
1.59429E+10
1.52571E+10
1.45714E+10
1.38857E+10
1.32E+10
1.25143E+10
1.18286E+10
1.11429E+10
1.04571E+10
9.77143E+09
9.08571E+09
8.4E+09
7.71429E+09
7.02857E+09
6.34286E+09
5.65714E+09
4.97143E+09
4.28571E+09
3.6E+09
2.91429E+09
2.22857E+09
1.54286E+09
8.57143E+08
1.71429E+08
-5.14286E+08
-1.2E+09
-1.88571E+09
-2.57143E+09
-3.25714E+09
-3.94286E+09
-4.62857E+09
-5.31429E+09
-6E+09

(3) 3 μs   (4) 4 μs

(5) 5 μs   (6) 6 μs

(7) 7 μs   (8) 8 μs

**Figure 5**. The results of eight different time intervals of MCSPH simulation (Upper halves) in comparison with AUTODYN Free Lagrange solver of Howell et al. [25] (Lower Halves). Pressure contour intervals of 1.0 (*GPa*) is selected in Howell et al. [25] work and the pressure field of MCSPH is shown in pictures

**TABLE 2.** Results for Al–Al impact at 3.1 *km/s*.

| Method | $P_1$ (*Gpa*)[a] | $P_2$ (*Gpa*)[b] | $d_{cra}$ (*cm*)[c] | $L_{extn}$ (*cm*)[d] | $L_{proj}$ (*cm*)[e] |
|---|---|---|---|---|---|
| *SAV1* | 18.0 | -18.5 | 2.0 | 0.7 | 1.8 |
| *SAV2* | 17.5 | -17.5 | 1.9 | 0.7 | 1.8 |
| *BAL* | 17.5 | -18.5 | 2.0 | 0.7 | 1.8 |
| *MON* | 22.0 | -13.5 | 2.0 | 0.8 | 2.0 |
| *CON* | 17.5 | -14.0 | 2.1 | 0.7 | 1.9 |
| *HB*[f] | 18.6 | -15.9 | 1.9 | 0.7 | 2.0 |
| *MCSPH*[g] | 18.72 | -16.62 | 1.92 | 0.7 | 1.83 |

**a.** Pressure generated at the centre of the projectile 1.0 (*μs*) after initial contact.
**b.** Peak tension generated in the projectile after the reflection of initial pressure wave, ~ 2.2(*μs*) after initial contact.
**c.** Crater diameter.
**d.** $L_{extn}$= Longitudinal extension of the projectile 8.0 (*μs*) after impact.
**e.** $L_{proj}$=Longitudinal distance traveled by the projectile in the 8.0 (*μs*) interval after impact.
**f.** Results from the free Lagrange solver of Ball and Howell.
**g.** Results from Modified Compressible SPH (MCSPH) implemented in current study.

The presented results show that this method has no tensile instability in comparison with SPH solver of AUTODYN [25] and standard SPH with artificial stress, Morris et al. [16], and only the thin region around the projectile shows a little discontinuity in about 8.0 (*μs*), which may be an effect from the number of particles used to solve this problem. The number of particles used in this study is 12046, while in the case of Mehra et al. [16] is 17850 and it can be a benefit of MCSPH method that can adequately simulate high velocity impacts with lower number of particles.

Clumping of particles in high tension regions always leads to unwanted results in problems involving high stress and pressure field with shock capturing or in tensile tests [22]. As shown in Figure 5, during the solution of the current presented algorithm, there is no clumping in particles in highly tensional zones and the algorithm shows acceptable results in tensional regions.

In Fig. 6, the results of high velocity impact case are compared with thosegiven by Mehra et al. [16] at 8.0 (*μs*). Results give the required assurance when are compared with other SPH methods; however in this study, the artificial viscosity is eliminated. As evident in Figure 6, the

results from MCSPH in case of shape are very similar to Contact algorithm and in case of magnitude are quite close to Howell et al. [25], expect for $L_{projec}$. Besides, as mentioned before, there is no major clumping in particles in 8.0 ($\mu s$) and it can be a valuable benefit of using MCSPH.

Another advantage of this method in comparison with other valuable SPH methods [16] is again a much lower tensile instability or numerical fracture.

Considering the fact that SPH techniques may have some inherent numerical fracture because of their particle nature and their discretizing techniques of principal equations, Howell et al. [25] with their free Lagrange method may have more reliable results than SPH ones. Consequently each method which has a closer result to Howell et al. [25] could be a more reliable SPH method than the others. So MCSPH can be a useful technique with a low numerical fracture and clumping for solving other problems with high tensional regions and large deformations and high velocities. It can be a future work to lessen its errors and progress it into other problems.

To give a comparison in case of magnitude of parameters, Table 2 denotes the geometric characters and the pressure values for current and other method. As Table 2 shows, in peak pressure $P_1$, current study shows a value close to Howell et. al. [25] as discussed before, but it also shows maximum tension $P_2$ as a moderate value in comparison with other techniques and also in the vicinity of Howell et al. [25]. Regarding the fact that all the results are numerical and there are no experimental results for this case, it is impossible to say which method has more accuracy indeed. But as Table 2 shows, for example, in the case of MON, considering the value of peak pressure $P_1$ and the value of maximum tension $P_2$ and clumping in particles and discontinuities in both the projectile and the target in Figure 6, it is obvious that MON method suffers from a big numerical fracture. In other SPH studies in Figure 6, CON has the best results in the simulated shape. Besides MCSPH is very much like CON in simulated shape and in case of magnitude its results is comparable with Howell et al. [25].
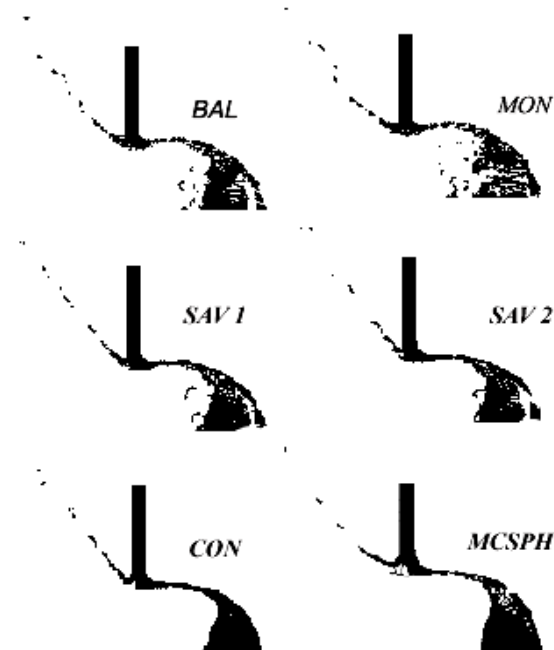
## 8. EFFECTS OF PARTICLE INITIAL LENGTH ON SIMULATIONS

To have an evident sense of resolution effects on simulations, three different particle initial lengths ($\Delta L$= 0.18 mm, 0.12 mm and 0.085 mm) are elected in high velocity case. This choice came from this theory in which the higher initial impact speeds are specified the higher tensile instabilities may occur. So, it will help one to have more reasonable vision of particle size on the simulations of MCSPH method.

Final stage geometrical parameters (at 8.0 $\mu s$) have been tabulated in Table 3. Results show a close compatibility in three resolutions. Decreasing the particle numbers will result in increasing the $P_1$ and the difference between P1 and $P_2$. In attention to Smoothing method which SPH methods use in their calculations, it would be expected that more particles result in more smoother and better values for principal parameters such as pressure. But the differences are not of a significant order and it is possible to say MCSPH is independent of particle size in general.

To prove this idea, 4 different depictions of simulations in different time intervals and in



**Figure 6.** The upper half figure of the impact for six different SPH solutions with initial projectile velocity of 3.1 *km/s* at 8.0 ($\mu s$) after the initial contact.

diverse ΔL are shown in Figure 7. As it is obvious, simulations are very similar and just in lower number of particles (ΔL=0.18 *mm*), MCSPH will encounter with some numerical instabilities in the region between projectile and target (in front of the projectile in 6 and 8 *μs*).

But this fact leads one to use a moderate number of particles in MCSPH method to prevent the probably numerical instabilities and time coasting in low particle numbers.

**TABLE 3.** Results for Al–Al impact at 3.1 *km/s* in three different ΔL

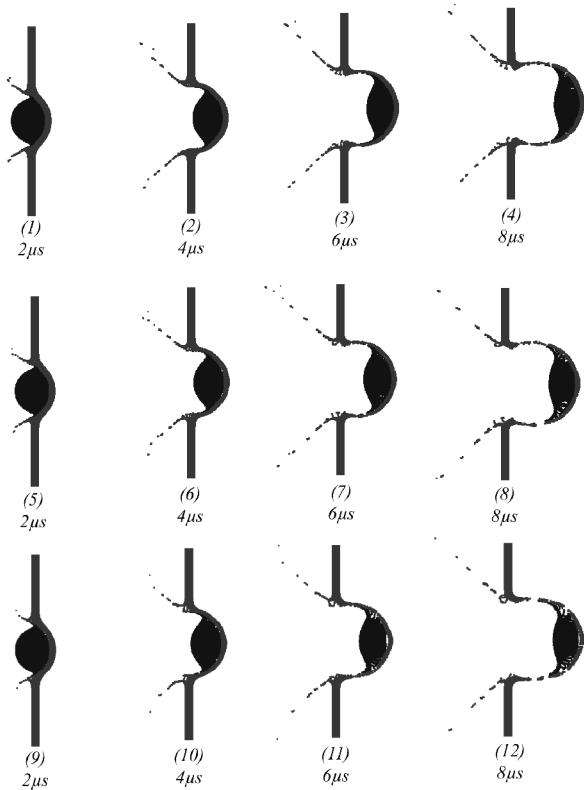| ΔL (mm) | $P_1$ (Gpa) | $P_2$ (Gpa) | $d_{cra}$ (cm) | $L_{proj}$ (cm) |
|---|---|---|---|---|
| *0.18* | 19.45 | -17.2 | 1.90 | 1.89 |
| *0.12* | 18.72 | -16.62 | 1.92 | 1.83 |
| *0.085* | 18.43 | -16.9 | 1.91 | 1.82 |



**Figure 7.** Results of the MCSPH simulations in 3 different ΔL. Figures 1 to 4 are related to ΔL = 0.18 *mm*, Figure 5 to 8 are related to ΔL =0.12 *mm* and Figures 9 to 12 are related to ΔL =0.085 *mm*.

# 9. CONCLUSION

In the current work, new proposed modified compressible algorithm of SPH method (MCSPH) is introduced which can simulate problems involving shock wave structures without need to include artificial viscosity. It is the result of the approach in which momentum equation is segregated into three parts and pressure is derived from an equation of state (EOS). To show its capabilities, two different 2D test cases were simulated by means of MCSPH method. The first one was a low velocity impact of an aluminum projectile to an aluminum target. The results were checked with Howell et al. [25] free Lagrange solver and SPH method, and shown good agreement with them in behavior of shock waves and magnitude of total x-wise stress $\sigma_{xx}$, x-wise velocity, pressure and density. Considering the behavior of the MCSPH that shown no numerical fracture or clumping, and with the compatibility of its results with the work of Howell et al. [25], and regarding the elimination of artificial viscosity as a controller of numerical oscillations, the MCSPH method sounds a much simpler SPH method with the adequate accuracy.

In the second test case, a high velocity impact of a spherical projectile to a thin semi infinite aluminum target is considered in 2 dimensions and is compared with Howell et al. [25] and 4 different SPH methods of Mehra et al. [16]. In this case, the magnitude of results complies with Howell et al. [25] as the most reliable work in this test case and the simulated shape has a good similarity with both Howell et al. [25] and CON with very low numerical fracture and clumping. Consequently, this research may provide the following conclusions about MCSPH:

1. The method simplifies the SPH algorithm by removing the artificial viscosity and using the three step algorithm.
2. Removing the artificial viscosity may lower the programming and computational efforts.
3. The method as a new algorithm has the capability of shock capturing as well as removing the artificial viscosity and using the three step procedure.

The method has the required assurance to be used and tested for both low and high velocity elastic-plastic deformations that covers a wide range of

continuum deformations, for example from a simple elastic vibration to fluidized behaviors in explosive welding.

## 10. REFERENCES

1.  Lucy, L.B., "A numerical approach to the testing of the fission hypothesis", *Astron Journal,* Vol. 82, (1977), 1013-1020.
2.  Benz, W., Smooth particle hydrodynamics: a review. In: Numerical Modeling of Non-linear Stellar Pulsation: Problems and Prospects, Kluwer Academic, Boston, MA, (1990), pp.269-288.
3.  Stamatellos, D., Whitworth, A. P., Bisbas, T. and Goodwin, S., "Radiative transfer and the energy equation in SPH simulations of star formation", *Astronomy and Astrophysics,* Vol. 475, Issue 1, (2007), pp.37-49
4.  Gesteira, M. G., Rogers, B. D., Dalrymple, R. A. and Crespo, A.J.C., "State-of-the-art of classical SPH for free-surface flows", *Journal of Hydraulic Research,* Vol. 48, (2010), 6–27
5.  Johnson, G.R., Petersen, E.H. and Stryk, R.A., "Incorporation of an SPH option into the EPIC code for a wide range of high velocity impact computations", *International Journal of Impact Engeineering*, Vol. 14, (1993), 385-394.
6.  Maruzewski, P., Le Touze, D., Oger, G. and Avellan, F., "SPH high-performance computing simulations of rigid solids impacting the free-surface of water", *Journal of Hydraulic Research,* Vol. 47, (2009), 126–134.
7.  Benz, W. and Asphaug, E., "Impact simulation with fracture, I. Method and tests", *Icarus, International journal of solar system studies,* Vol. 107, (1994), 98-116.
8.  Monaghan, J.J., "Smoothed particle hydrodynamics", *Annual Review of Astronomy and Astrophysics*, Vol. 30, (1992), 543-574.
9.  Gingold, R.A. and Monaghan, J.J., "Smoothed particle hydrodynamics: Theory and application to nonspherical stars", *Monthly Notices of Royal Astronomical Society,* Vol. 181, (1977), 275-389.
10. Hongbin, J. and Xin, D., "On criterions for smoothed particle hydrodynamics kernels in stable field", *Journal of Computational Physics*, Vol. 202, No. 2, (2004), 699-709.
11. Monaghan, J.J. and Gingold, R.A., "Shock simulation by the particle method SPH", *Journal of Computational Physics,* Vol. 52, (1983), 347-389.
12. Monaghan, J.J., "Extrapolating b-splines for interpolation", *Journal of Computational Physics*, Vol. 60, No. 2, (1985), 253-262.
13. Gingold, R.A. and Monaghan, J.J., "Kernel estimates as a basis for general particle methods in hydrodynamics", *Journal of Computational Physics,* Vol. 46, (1982), 429-453.
14. Morris, J.P., Fox, P.J. and Zhu, Y., "Modeling low Reynolds number incompressible flows using SPH", *Journal of Computational Physics*, Vol. 136, (1997), 214-226.
15. Hosseini, S.M., Manzari, M.T. and Hannani, S.K., "A fully explicit three-step SPH algorithm for simulation of non-Newtonian fluid flow", *Journal of Numerical Methods for Heat and Fluid Flow*, Vol. 17, (2007), 715-735.
16. Mehra, V. and Chaturvedi, S., "High velocity impact of metal sphere on thin metallic plates, a comparative smooth particle hydrodynamics study", *Journal of Computational Physics*, Vol. 212, (2006), 318-337.
17. Monaghan, J.J., "Smoothed Particle Hydrodynamics", *Reports on Progress in Physics,* Vol. 68, (2005), 1703-1759.
18. Hosseini, S.M. and Amanifard, N., "Presenting a Modified SPH Algorithm for Numerical Studies of Fluid-Structure Interaction Problems", *International Journal of Engineering, Trans B: Applications*, Vol. 20, (2007), pp.167-178.
19. Farahani, M.H. and Amanifard, N.," A high velocity impact simulation using SPH projection method", *International Journal of Engineering, Trans B: Applications,* Vol. 22, No. 4, (2009), 359-368.
20. Liu, G. R. and Liu, M. B., "Smoothed Particle Hydrodynamics a mesh free particle method", *World Scientific Publishing,* (2003), 125-127.
21. Monaghan, J.J. and Poinracic, J., "Artificial viscosityfor particle methods", *Applied Numerical Mathematics*, Vol. 1, (1985), 187-194.
22. Gray, J.P., Monaghan, J.J. and Swift, R.P, "SPH elastic dynamics", *Computer Methods in Applied Mechanic and Engineering*, Vol. 190, (2001), 6641-6662.
23. Shintate, K. and Sekine, H., " Numerical simulation of hypervelocity impacts of a projectile on laminated composite plate targets by means of improved SPH method", *J. Composites*, *Part A*, Vol. 35, (2004), 683–692.
24. Benz, W. and Asphaug, E., "Simulation of brittle solids using smooth particle hydrodynamics", *Journal of Computer and Physics communications*, Vol. 87, (1995), 253-265.
25. Howell, B.P. and Ball, G.J., "A free-lagrange augmented Godunov method for the simulation of elastic-plastic solids", *Journal of Computational Physics*, Vol. 175, (2002), 128-167.